

# Metamaterial-Based Low-Profile Broadband Aperture Coupled Grid-Slotted Patch Antenna

Wei Liu, Zhi Ning Chen, and Xianming Qing

**Abstract**—A metamaterial-based broadband low-profile grid-slotted patch antenna is presented. By slotting the radiating patch, a periodic array of series capacitor loaded metamaterial patch cells is formed, and excited through the coupling aperture in a ground plane right underneath and parallel to the slot at the center of the patch. By exciting two adjacent resonant modes simultaneously, broadband impedance matching and consistent radiation are achieved. The dispersion relation of the capacitor-loaded patch cell is applied in the mode analysis. The proposed grid-slotted patch antenna with a low profile of  $0.06 \lambda_0$  ( $\lambda_0$  is the center operating wavelength in free space) achieves a measured bandwidth of 28% for the  $|S_{11}|$  less than  $-10$  dB and maximum gain of 9.8 dBi.

**Index Terms**—Broadband antenna, low profile, metamaterial, patch antenna, capacitor-loaded patch cell, aperture coupling, transmission-line model, wide bandwidth.

## I. INTRODUCTION

With the advancement of modern wireless communication systems, broadband antennas are of increasing demand. Microstrip patch antennas have been received much attention because of their low profile, light weight, low cost, compatible with printed circuits, although they suffer from narrow impedance bandwidth. Many techniques have been reported to overcome the drawback of the inherent narrow bandwidth, including the utilization of capacitive probe feed, L-probe feed, aperture coupling, U/E-slotted patch, and stacked patches [1–6]. However, a thick substrate with low dielectric constant is usually required and therefore it is difficult to make the antenna low-profile. We have proposed a unique broadband low-profile antenna design methodology using a composite right/left-handed (CRLH) mushroom structure [7–9]. The  $TM_{10}$  mode and antiphase  $TM_{20}$  mode are simultaneously excited with similar boresight radiation patterns. The distinguished operating principle enables the utilization of a substrate with small thickness and relatively high permittivity for broadband antenna design. Note that in such a design the dual operating modes are both located on the right-handed (RH) dispersion branch of the CRLH mushroom structure. The left-handed (LH) branch is not necessary for such dual-mode antenna [10].

In this paper, we present a broadband low-profile metamaterial-based grid-slotted microstrip patch antenna. The aperture coupled feeding structure on the ground plane is positioned right underneath and parallel to the grid slot at the center of the patch. The radiating grid-slotted patch can be considered as a periodic structure comprising series capacitor loaded metamaterial patch cells, which produce a pure RH dispersion branch with a zero phase constant at a finite and non-zero frequency. The  $TM_{10}$  mode and antiphase  $TM_{20}$  mode are excited in the grid-slotted patch antenna as well. Based on the dispersion relation of the capacitor-loaded patch unit cell, the effects of the variation of the slot grid and the overall patch on the antenna performance are investigated. The proposed antenna is numerically studied by using CST Microwave Studio [11] and experimentally validated.

Manuscript received November 24, 2011; revised March xx, 2015. This work was supported by MOE AcRF Tier 1 Project of “Study of metadielectric and its applications” (STARTUP GRANT).

W. Liu and Z. N. Chen are with Department of Electrical & Computer Engineering, National University of Singapore, 117583 Singapore (e-mail: eleliw@nus.edu.sg, eleczn@nus.edu.sg).

Z. N. Chen and X. Qing are with the Institute for Infocomm Research (I<sup>2</sup>R), Agency for Science, Technology and Research (A\*STAR), 138632 Singapore (e-mail: chenzn@i2r.a-star.edu.sg, qingxm@i2r.a-star.edu.sg).

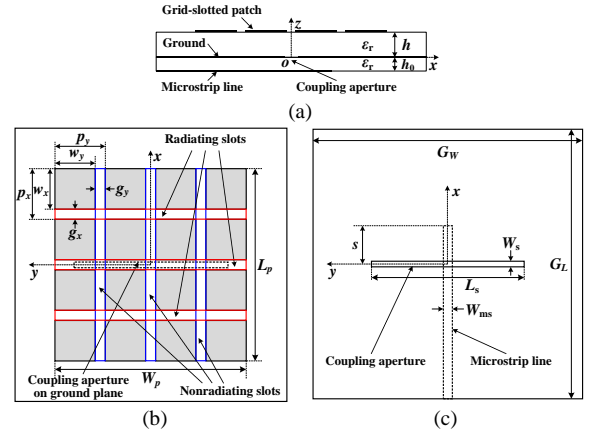


Fig. 1. Geometry of the proposed aperture coupled grid-slotted patch antenna and the coordinate system: (a) side view, (b) top view of the grid-slotted patch, and (c) top view of the microstrip-line aperture coupling structure.

TABLE I  
DIMENSIONS OF THE GRID-SLOTTED PATCH ANTENNA (UNIT: mm)

$p_x$	$g_x$	$p_y$	$g_y$	$n_x$	$n_y$	$L_p$	$W_p$
10	1	10	1	3	3	39	39
$h$	$h_0$	$L_s$	$W_s$	$s$	$W_{ms}$	$G_L$	$G_W$
3.25	0.813	26	2	9	1.85	60	60

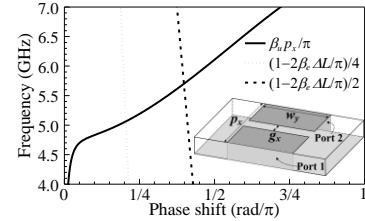


Fig. 2. Dispersion diagram of the series-capacitor-loaded patch unit cell.

## II. GRID-SLOTTED PATCH ANTENNA

The proposed metamaterial-based grid-slotted patch antenna is shown in Fig. 1. It is a three-layer structure where the upper and lower dielectric substrates are Rogers RO4003C with the relative permittivity of 3.38, loss tangent of 0.0027, and respective thickness of  $h$  and  $h_0$ . The rectangular microstrip patch ( $L_p \times W_p$ ) printed onto the top layer of the upper substrate ( $G_L \times G_W$ ) is cut up by a uniform slot grid. The number and width of the grid slots in the resonant and non-resonant direction are  $(n_x, g_x)$  and  $(n_y, g_y)$ , respectively. The grid-slotted patch can be considered as a two-dimensionally periodic structure of capacitor-loaded patch unit cells with a number, period and patch width of  $(m_x, p_x, w_x)$  and  $(m_y, p_y, w_y)$  along  $x$ - and  $y$ -axis direction, separately, and  $m_x = n_x + 1$ ,  $m_y = n_y + 1$ ,  $p_x = w_x + g_x$ ,  $p_y = w_y + g_y$ ,  $L_p = m_x p_x - g_x$ ,  $W_p = m_y p_y - g_y$ . The antenna is center-fed by a  $50\text{-}\Omega$  microstrip line through an aperture cut in the ground plane. The slot number  $n_x$  should be odd to align the coupling aperture to the center grid slot.

The optimized dimensions of a grid-slotted patch antenna are tabulated in Table I. The whole patch is cut into a  $4 \times 4$  patch array with three radiating slots and three non-radiating slots. The corresponding antenna performance is to be analyzed by considering the dispersion property of the capacitor-loaded patch unit cell. The connecting via of the unit cell is removed when compared with the metamaterial mushroom antenna [7], leading to the absence of the LH branch and preservation of the RH dispersion characterized with a zero phase constant at a specific non-zero frequency. The aperture coupled grid-slotted patch sustains  $TM_{10}$  and antiphase  $TM_{20}$  modes closely spaced at the RH dispersion branch as well. The transmission-line

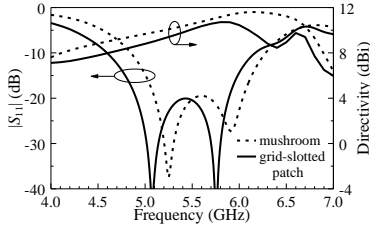


Fig. 3. Simulated  $|S_{11}|$  and boresight directivity of grid-slotted patch antenna.

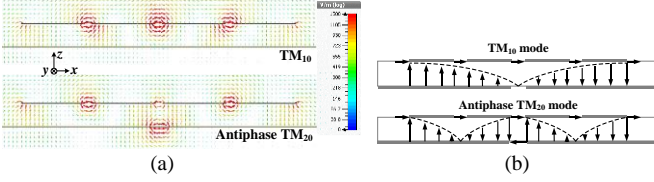


Fig. 4.  $TM_{10}$  and antiphase  $TM_{20}$  mode of the equally grid-slotted patch antenna: (a) simulated electric field distribution on  $y = 5$  mm plane at 5.07 GHz and 5.76 GHz, and (b) sketch of the operation mechanism.

model is still applicable to the mode analysis of the vialess grid-slotted patch antenna, and the equations for estimating the dual-mode frequencies [7], [12] are reproduced as following:

$$\beta_u p_x / \pi = \frac{1 - 2\beta_e \Delta L / \pi}{m_x}, TM_{10} \text{ mode} \quad (1)$$

$$\beta_u p_x / \pi = \frac{1 - 2\beta_e \Delta L / \pi}{m_x / 2}, \text{antiphase } TM_{20} \text{ mode} \quad (2)$$

$$\beta_e = 2\pi f \sqrt{\epsilon_{re}} / c \quad (3)$$

$$\frac{\Delta L}{h} = 0.412 \frac{(\epsilon_{re} + 0.3)(W_p/h + 0.262)}{(\epsilon_{re} - 0.258)(W_p/h + 0.813)} \quad (4)$$

$$\epsilon_{re} = \frac{\epsilon_r + 1}{2} + \frac{\epsilon_r - 1}{2} (1 + 12h/W_p)^{-1/2} \quad (5)$$

where  $f$  is the operating frequency,  $c$  is the speed of light in vacuum,  $\beta_u$  is the propagation constant of the capacitor-loaded patch unit cell, and  $\beta_e$  is the propagation constant in the effective extended region with a length of  $\Delta L$  at each end along the resonant direction due to the effect of the fringing field.

Fig. 2 shows the dispersion diagram of the capacitor-loaded patch unit cell obtained from full-wave simulation. The simulation model of the unit cell is shown in the inset of Fig. 2. The right-hand side terms of (1) and (2) are also plotted in Fig. 2 for determining the resonant frequencies of the operating  $TM_{10}$  and antiphase  $TM_{20}$  modes. The predicted resonant frequencies of the dual modes based on the transmission-line model are 5.06 GHz and 5.70 GHz respectively. Fig. 3 presents the simulated  $|S_{11}|$  and boresight directivity of the antenna. Two resonances appear at the frequencies of 5.07 GHz and 5.76 GHz, which are close to the prediction. Fig. 4(a) shows the simulated  $E$ -field distributions on the plane of  $y = 5$  mm at 5.07 GHz and 5.76 GHz, in correspondence to the  $TM_{10}$  and antiphase  $TM_{20}$  mode respectively. In the antiphase  $TM_{20}$  mode, the directions of the  $E$ -field at the opposite sides of the central aperture-slot region are antiparallel. In-phase radiation field distributions along the radiating slots and the open edges are excited for both the  $TM_{10}$  and antiphase  $TM_{20}$  mode as illustrated in Fig. 4(b). The closely-spaced dual modes result in broadband performance.

As shown in Fig. 3, the proposed grid-slotted patch antenna achieves a  $-10$ -dB impedance bandwidth of 29% ranging from 4.60 GHz to 6.17 GHz. Over the bandwidth, the boresight directivity varies from 8.0 dBi to 10.7 dBi. The performance of the reference mushroom antenna is compared in Fig. 3 as well. The reference mushroom antenna has a center-connected shorting via with a diameter of 0.6 mm

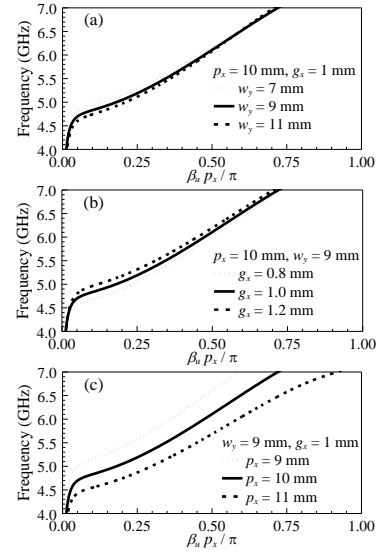


Fig. 5. Dispersion diagram of capacitor-loaded patch unit with different (a)  $w_y$ , (b)  $g_x$ , and (c)  $p_x$ .

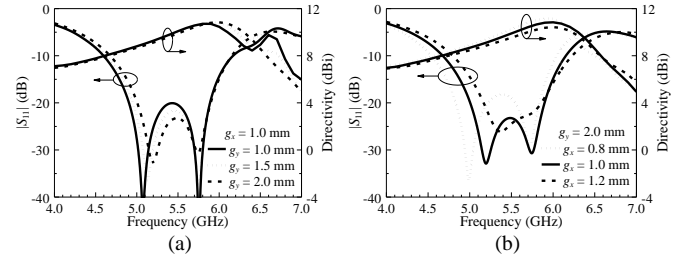


Fig. 6.  $|S_{11}|$  and boresight directivity with different (a)  $g_y$ , and (b)  $g_x$ .

for each mushroom cell, and a coupling aperture of  $30 \text{ mm} \times 1.6 \text{ mm}$  [7]. The other dimensions are the same as the grid-slotted patch antenna. The mushroom antenna attains a boresight directivity of 9.4–11.6 dBi over the  $-10$ -dB impedance bandwidth of 4.85 GHz–6.28 GHz or 26%. The grid-slotted patch antenna can be regarded as a specific mushroom antenna with a shorting via diameter of zero. With the decrease of the shorting via diameter, the increasing effective shunt inductance in the unit cell lowers both the resonant frequencies and quality factor of the antenna. Compared with the mushroom antenna counterpart, the vialess grid-slotted patch antenna achieves a wider operating bandwidth of 29% and a lower center frequency of 5.385 GHz with the same levels of in-band return loss.

### III. PARAMETRIC STUDIES

Since the dominant surface wave launched in the grounded substrate is along the  $E$ -plane of the grid-slotted patch antenna over the operating band [9], the antenna performances are affected by the ground substrate length  $G_L$ , whereas, they are hardly influenced by  $G_W$ . The optimized ground substrate of  $60 \text{ mm} \times 60 \text{ mm}$  is fixed for the proposed antenna by taking into account the reflection coefficient, gain, and backlobe levels. In this section, the effects of the variation in the slot grid on the performance of the proposed grid-slotted patch antenna are firstly examined with a fixed overall patch of  $39 \text{ mm} \times 39 \text{ mm}$ . Then, the effect of the size of the overall microstrip patch on the antenna performance is studied. Finally, the analysis of the unequally grid-slotted patch antenna is carried out. As the dispersion property of the constituent capacitor-loaded patch cell plays a key role in the antenna performance, the changes in the dispersion diagram of the unit cell by varying the parameters  $p_x$ ,  $w_y$  and  $g_x$  are extracted as shown in Fig. 5. The proposed antenna with the dimensions listed in Table I is

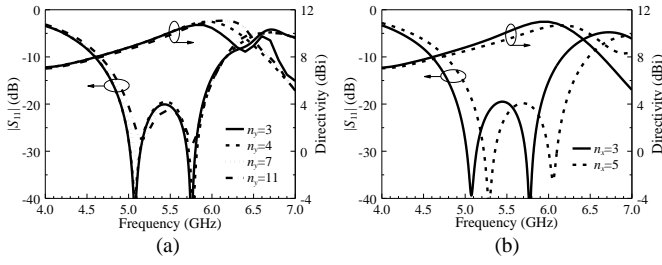


Fig. 7.  $|S_{11}|$  and boresight directivity with different (a) non-radiating slot number  $n_y$ , and (b) radiating slot number  $n_x$  ( $n_x = 3, n_y = 4, g_x = 1$  mm,  $L_x = 26$  mm,  $s = 9$  mm;  $n_x = 5, n_y = 4, g_x = 0.3$  mm,  $L_x = 24$  mm,  $s = 8.5$  mm).

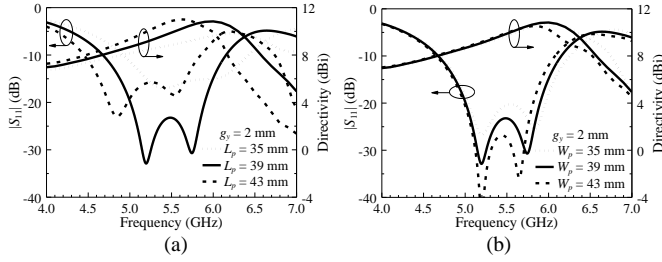


Fig. 8.  $|S_{11}|$  and boresight directivity with different (a)  $L_p$ , and (b)  $W_p$ .

used as reference, and only the parameters with different values are to be addressed in the plots of the following parametric study.

#### A. Grid Slot Width ( $g_x, g_y$ )

The influence of different nonradiating slot width,  $g_y$ , on the  $|S_{11}|$  and directivity is shown in Fig. 6(a). The other dimensions are kept the same as the reference antenna. The increase of  $g_y$  corresponds to the decrease of patch width  $w_y$ . With the decrease of  $w_y$ , the lower part of the RH dispersion branch is shifted to higher frequencies while the higher part around  $\beta_y p_x = \pi/2$  is almost unchanged as shown in Fig. 5(a). The change tendency of the dispersion relation indicates that the  $TM_{10}$  mode resonant frequency increases with the increment of  $g_y$  while the antiphase  $TM_{20}$  mode resonant frequency is hardly affected, as shown in Fig. 6(a). It is also seen from the directivity curves that the directivity degradation at the higher frequencies, resulting from the higher order mode along the non-resonant direction, is improved when  $g_y$  increases from 1.0 mm to 2.0 mm.

The effect of the radiating slot width,  $g_x$ , on the dispersion relation is examined with  $g_y = 2.0$  mm. From the RH dispersion branch as shown in Fig. 5(b), the frequencies become lower when  $g_x$  changes from 1.2 mm to 0.8 mm. Therefore, the operating band of the antenna shifts to lower frequencies with the decrement of radiating slot width as reflected in Fig. 6(b). The directivity increases with a more uniform field distribution on the antenna surface because of the smaller radiating slot width.

#### B. Grid Slot Number ( $n_x, n_y$ )

Fig. 7(a) shows the  $|S_{11}|$  and directivity of the antenna with increasing nonradiating slot number  $n_y$ . As the overall patch is equally cut up by the slot grid, the increase in  $n_y$  corresponds to the decrease in  $w_y$ . Therefore, similar results are found both with increasing the width  $g_y$  and number  $n_y$  of the nonradiating slots. The higher order mode along the non-resonant direction is eliminated from the operating bandwidth as well by cutting more nonradiating slots.

Consider five radiating slots etched on the overall patch to check the effect of the radiating slot number  $n_x$  on the antenna performance. Four nonradiating slots are used in both antennas with  $n_x = 3$  and  $n_x = 5$ . For the antenna with five radiating slots, smaller radiating slot width  $g_x$  of 0.3 mm is used to sustain a uniform field distribution on the top surface with the optimized feed dimensions of  $L_s = 24$  mm and  $s = 8.5$  mm.

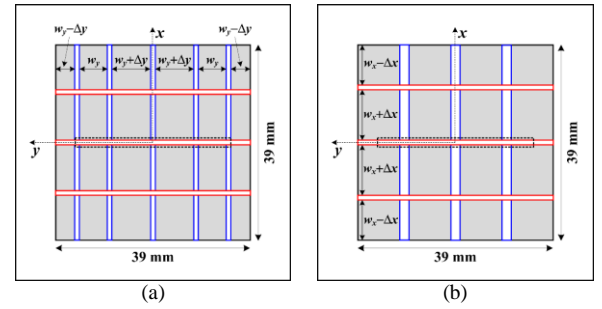


Fig. 9. Unequally grid-slotted patch antenna: (a) non-uniform distributed nonradiating slots, (b) non-uniform distributed radiating slots.

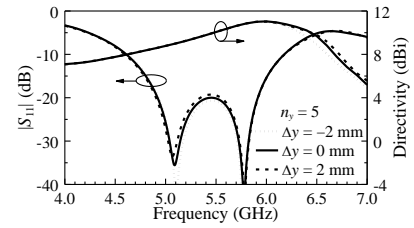


Fig. 10.  $|S_{11}|$  and boresight directivity of the antenna unequally slotted along non-resonant direction.

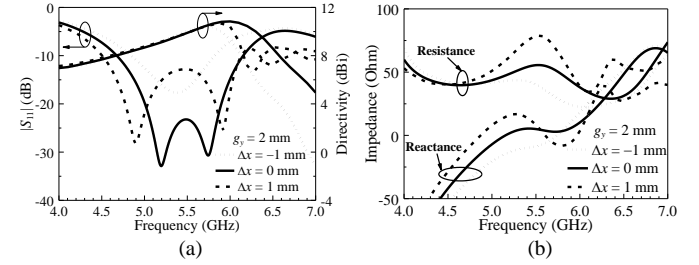


Fig. 11. The antenna unequally slotted along resonant direction: (a)  $|S_{11}|$  and boresight directivity, and (b) input impedance.

The  $|S_{11}|$  and directivity of the proposed antenna with  $n_x = 5$  and  $n_x = 3$  are compared in Fig. 7(b). Almost the same fractional bandwidth for both return loss and directivity is achieved with more radiating slots of smaller width.

#### C. Size of Overall Patch ( $L_p, W_p$ )

The size of the overall patch on the antenna performance is studied, where the patch is equally cut up by a slot-grid with  $g_y = 2$  mm. When the length of the constituent unit cell  $p_x$  increases, the whole RH dispersion branch shifts down to lower frequencies as shown in Fig. 5(c). Therefore, the increment of the overall patch length  $L_p$  results in a considerable downshift in the operating bandwidth of the antenna as plotted in Fig. 8(a). The directivity increases with a longer patch because of the enlarged effective radiating aperture.

Fig. 8(b) shows the  $|S_{11}|$  and directivity with varying overall patch width  $W_p$ . When the overall patch width  $W_p$  increases from 35 mm to 43 mm, the upper resonant frequency decreases from 5.84 GHz to 5.65 GHz, while the lower resonant frequency is hardly affected.

#### D. Unequally Grid-Slotted Patch ( $\Delta x, \Delta y$ )

The overall patch of all the aforementioned antennas is equally cut up by a slot grid. Herein, we investigate the performance of the unequally grid-slotted patch antenna. As shown in Fig. 9(a), the antenna with five nonradiating slots symmetrically but unequally spaced along non-resonant direction is taken into account. As suggested from Fig. 10, the non-uniform distribution of the non-radiating slots has a slight effect on the impedance matching and directivity of the antenna.

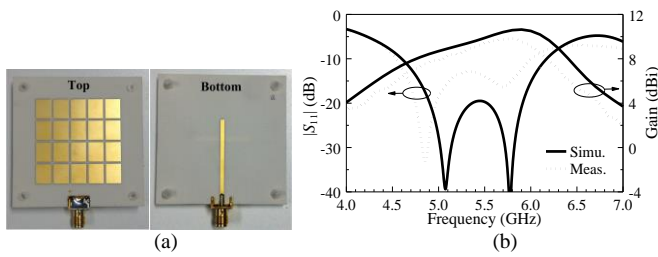


Fig. 12. (a) Photograph of antenna prototype, (b)  $|S_{11}|$  and gain.

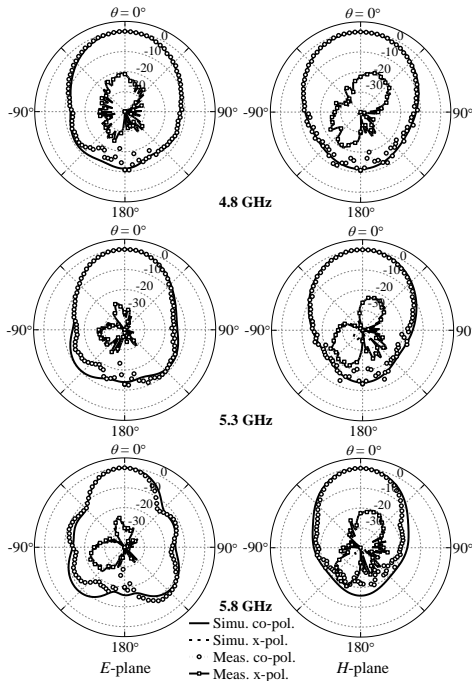


Fig. 13. Radiation patterns at 4.8 GHz, 5.3 GHz, and 5.8 GHz.

Consider the grid-slotted patch antenna unequally cut up by three radiating slots. Three nonradiating slots with  $g_y = 2$  mm are equally spaced along the non-resonant direction. The center radiating slot is still cut at the center of the overall patch. The two side radiating slots are shifted from the quarter-length positions as shown in Fig. 9(b). The impedance matching of the antenna is sensitive to shifting the side radiating slots as plotted in Fig. 11. As the side radiating slots moving to the edges, the input resistance increases and the input reactance exhibits larger ripple over the operating bandwidth, leading to a widened  $-10$ -dB impedance bandwidth but increased in-band return loss. The directivity at the higher part of the bandwidth is deteriorated when the side radiating slots are shifted away from the quarter-length positions.

#### IV. EXPERIMENTAL RESULTS

In order to validate the proposed antenna design, a microstrip-line aperture coupled equally grid-slotted patch antenna was prototyped and measured. The antenna prototype has the same dimensions as those listed in Table II, except the use of four nonradiating slots. Fig. 12(a) shows the prototype of the antenna with an overall size of  $60$  mm  $\times$   $60$  mm  $\times$   $4.1$  mm.

Fig. 12(b) illustrates the simulated and measured reflection coefficient and realized gain of the antenna. Over the simulated  $-10$ -dB impedance bandwidth of  $4.60$  GHz– $6.17$  GHz or  $29\%$ , the simulated gain ranges from  $7.4$  dBi to  $10.6$  dBi. The simulated radiation efficiency is higher than  $92\%$  over the bandwidth ranging from  $4.60$  GHz

to  $6.17$  GHz with a peak efficiency of  $97\%$  around  $5$  GHz. The measured  $-10$ -dB impedance bandwidth is from  $4.54$  GHz to  $6.00$  GHz or  $28\%$  with the measured gain ranging from  $6.0$  dBi to  $9.8$  dBi. Reasonable agreement is observed between the simulated and measured results. The slight downwards shift of the operating frequencies may come from the increased actual dielectric constant of the substrate, the fabrication and/or assemble tolerance of the antenna.

The simulated and measured radiation patterns of the antenna at  $4.8$  GHz,  $5.3$  GHz, and  $5.8$  GHz are exhibited in Fig. 13. The measured co-polarization patterns are in good coincidence with the simulation. The simulated cross-polarization levels are less than  $-130$  dB in the  $E$ -plane and  $-33$  dB in the  $H$ -plane. The measured cross-polarization levels are below  $-20$  dB in both the  $E$ - and  $H$ -planes. The discrepancy between the simulated and measured cross-polarization levels may be caused by the SMA connector and the measurement environment. In general, consistent boresight radiation with low cross-polarization level is achieved over the entire operating bandwidth.

#### V. CONCLUSION

A broadband low-profile aperture coupled metamaterial grid-slotted patch antenna has been proposed. Transmission-line model integrated with the dispersion relation of the constituent capacitor-loaded patch cells has been applied in the analysis of the dual operating modes. The effects of the variations in the overall patch and slot-grid on the antenna performance have been investigated. The backlobe levels can be further suppressed by using an aperture coupling structure with a shielding plane such as stripline and substrate integrated waveguide if required. This vialess compact broadband radiator can be employed in satellite, radar and wireless communication systems.

#### REFERENCES

- [1] P. S. Hall, "Probe compensation in thick microstrip patches," *Electron. Lett.*, vol. 23, no. 11, pp. 606–607, May 1987.
- [2] K. M. Luk, C. L. Mak, Y. L. Chow, and K. F. Lee, "Broadband microstrip patch antenna," *Electron. Lett.*, vol. 34, no. 15, pp. 1442–1443, Jul. 1998.
- [3] S. D. Targonski and D. M. Pozar, "Design of wideband circularly polarized aperture-coupled microstrip antennas," *IEEE Trans. Antennas Propag.*, vol. 41, no. 2, pp. 214–220, Feb. 1993.
- [4] K. F. Lee, K. M. Luk, K. F. Tong, S. M. Shum, T. Huynh, and R. Q. Lee, "Experimental and simulation studies of the coaxially fed U-slot rectangular patch antenna," *IEE Proc. Microwaves Antennas Propag.*, vol. 144, no. 5, pp. 354–358, Oct. 1997.
- [5] F. Croq and A. Papiernik, "Stacked slot-coupled printed antenna," *IEEE Microwave Guided Wave Lett.*, vol. 1, no. 10, pp. 288–290, Oct. 1991.
- [6] D. Sun, W. Dou, L. You, X. Yan, and R. Shen, "A broadband proximity-coupled stacked microstrip antenna with cavity-backed configuration," *IEEE Antennas Wireless Propag. Lett.*, vol. 10, pp. 1055–1058, Oct. 2011.
- [7] W. Liu, Z. N. Chen, and X. Qing, "Metamaterial-based low-profile broadband mushroom antenna," *IEEE Trans. Antennas Propag.*, vol. 62, no. 3, pp. 1165–1172, Mar. 2014.
- [8] W. Liu, Z. N. Chen, and X. Qing, "Stripline aperture coupled metamaterial mushroom antenna with increased front-to-back ratio," *IEEE International Symposium on Antennas and Propagation and USNC-URSI Radio Science Meeting*, Memphis, Tennessee, USA, Jul. 6–12, 2014, pp. 444–445.
- [9] W. Liu, Z. N. Chen, and X. Qing, "60-GHz thin broadband high-gain LTCC metamaterial-mushroom antenna array," *IEEE Trans. Antennas Propag.*, vol. 62, no. 9, pp. 4592–4601, Sep. 2014.
- [10] C. Caloz and T. Itoh, *Electromagnetic Metamaterials: Transmission Line Theory and Microwave Applications*. New York, NY, USA: Wiley, 2006.
- [11] CST Microwave Studio, *Computer Simulation Technology* [Online]. Available: <http://www.cst.com/Content/Products/MWS/Overview.aspx>.
- [12] E. O. Hammerstad, "Equations for microstrip circuit design," in *Proc. 5th Eur. Microwave Conf.*, Hamburg, West Germany, Sep. 1–4, 1975, pp. 268–272.